Solid State Ionics 254 (2014) 11–16

Contents lists available at ScienceDirect

Solid State Ionics

journal homepage: www.elsevier.com/locate/ssi

Oxygen vacancy formation energies in Sr-doped complex perovskites: *ab initio* thermodynamic study

Denis Gryaznov [a,d,*], Mike W. Finnis [b], Robert A. Evarestov [c], Joachim Maier [a]

[a] Max Planck Institute for Solid State Research, Heisenbergstr. 1, D-70569 Stuttgart, Germany
[b] Department of Materials, Imperial College London, Exhibition Road, London SW7 2AZ, UK
[c] Department of Quantum Chemistry, St. Petersburg University, Universitetsky Prosp. 26, 198504 St. Peterhof, Russia
[d] Institute for Solid State Physics, University of Latvia, Kengaraga 8, LV-1063 Riga, Latvia

ARTICLE INFO

Article history:
Received 3 December 2012
Received in revised form 21 October 2013
Accepted 22 October 2013
Available online xxxx

Keywords:
Density functional theory
Perovskite
Oxygen vacancy
Phonons

ABSTRACT

$La_{1-x}Sr_xCo_{0.25}Fe_{0.75}O_{3-\delta}$ is known as one of the best cathode materials for permeation membranes and solid oxide fuel cells. Optimization of its chemical composition is a challenging problem. One of the key properties is concentration of oxygen vacancies, which is controlled by their formation energies. *Ab initio* calculations were employed in order to study the formation of oxygen vacancies in $La_{1-x}Sr_xCo_{0.25}Fe_{0.75}O_{3-\delta}$ perovskites by varying the Sr content from x = 12.5% to 50%. The formation energies were obtained for different stoichiometries as functions of temperature and oxygen partial pressure. For this purpose we calculated the phonon frequencies in the solid phase and the chemical potential of oxygen. We have shown that the phonon contribution to the free energy of formation becomes increasingly important in $La_{1-x}Sr_xCo_{0.25}Fe_{0.75}O_{3-\delta}$ not only with rising temperature but also with rising Sr content. We find that the formation energies decrease significantly with increasing Sr content due to the phonon contribution. A simple explanation is proposed for the increasing role of phonons in the oxygen vacancy formation energies on the basis of phonon mode changes in comparison to defect-free materials. A careful analysis of the experimental results from the literature is also presented.

1. Introduction

Cobaltite based electrode materials, like $(La,Sr)(Co,Fe)O_3$ are extensively studied for applications in oxygen permeation membranes [1] and solid oxide fuel cells [2]. Such complex perovskite oxides form dense ceramic membranes having high ionic and electronic conductivity. Also, the quality of cathode material for solid oxide fuel cells is to a large extent determined by its stability in an oxidizing atmosphere and its level of catalytic activity for the oxygen reduction reaction [2].

The role of oxygen vacancies in these processes is crucial and a detailed understanding of the energetics of individual vacancies, based on *ab initio* calculations, would be of considerable help in predicting the stability and properties of the materials.

Recently, complex perovskite oxides have attracted great attention from the point of view of establishing efficient computation methods to calculate their electronic structure [3–10]. Many of these calculations deal with the behavior of point defects. The oxygen vacancy controls the mass transport at the high operating temperatures of solid oxide fuel cells; therefore, the inclusion of temperature in such computational methods is very important.

The inclusion of temperature implies at least the calculation of phonon frequencies and the temperature dependence of the oxygen chemical potential. Attempts to include the phonon contribution to the formation energies of oxygen vacancies in perovskite oxides are known from the literature. However, *ab initio* calculations of phonon frequencies in large unit cells with defects are often very time consuming. This is why Lee et al. [11] used a simple Einstein model to estimate the oxygen vibrational contribution in $LaMnO_3$ and Sundell et al. [12] calculated the phonon contributions of just the neighboring oxygen atoms around an oxygen vacancy in $BaZrO_3$. Wessel et al. [9] calculated the thermodynamic stability of the cubic phase in doped and undoped $(Ba,Sr)(Co,Fe)O_3$ by calculating the full phonon contribution to the free energies. Recently, we performed similar calculations for structural phase transitions in $SrTiO_3$ and $BaTiO_3$ [13,14], phonon properties in $LaCoO_3$ [15] and the phonon contribution to the formation energy of an oxygen vacancy in $SrTiO_3$ [16]. Notice that the phonon frequencies in $LaCoO_3$ [15] are not well reproduced in comparison to the experiments using the so-called DFT + U approach in contrast to other properties. In comparison to $SrTiO_3$, a higher oxygen vacancy concentration is expected in $(La,Sr)(Co,Fe)O_3$ in particular with high Sr content. It is the aim of the present study to analyze the phonon properties in such complex systems and to estimate the phonon contribution to the formation energy of an oxygen vacancy quantitatively. We will explain how the lattice vibrations contribute to decreasing formation energies of oxygen vacancies in $(La,Sr)(Co,Fe)O_3$ with increasing Sr content and demonstrate the effect of phonon mode changes in the presence of oxygen vacancies. In addition, we have addressed symmetry aspects important

* Corresponding author. Tel.: +49 7116891771.
E-mail addresses: d.gryaznov@fkf.mpg.de, gryaznov@mail.com (D. Gryaznov).

0167-2738/$ – see front matter © 2013 Published by Elsevier B.V.
http://dx.doi.org/10.1016/j.ssi.2013.10.046

for the choice of superstructures to model such complex systems. Stable superstructures must be selected in order to allow one to calculate the real phonon frequencies needed for a thermodynamic analysis.

Section 2 is devoted to symmetry considerations of the possible superstructures for $La_{1-x}Sr_xCo_{0.25}Fe_{0.75}O_{3-\delta}$ that we have treated, based on a supercell of 2×2×2 unit cells of cubic perovskite. Sections 3 and 4 describe computational methods and main results for oxygen vacancy behavior in $La_{1-x}Sr_xCo_{0.25}Fe_{0.75}O_{3-\delta}$. In Section 5 we present main conclusions.

2. Structure and symmetry of models

The modeling of defective crystals for different defect concentrations is performed with periodic boundary conditions based on the supercell approach [17]. Let us suppose that Co atoms substitute for Fe in the cubic perovskite structure of $LaFeO_3$, and the atomic fraction of Co is 0.25. This requires a 2×2×2 extension of the primitive unit cell giving 40 atoms in the supercell, i.e. 8 La, 8 Fe and 24 O atoms. There are three ways to arrange two Co atoms (Fig. 1) and to occupy symmetry-equivalent Fe sites in this cubic structure. Two arrangements of Co atoms in Figs. 1a and b are stable with respect to the formation of anti-phase boundaries [18,19] whereas the one in Fig. 1c is not stable, according to the so-called Lifshitz criterion [20]. We refer to a superstructure containing the sublattice in Fig. 1c in the following for comparison and emphasize its importance for our thermodynamic considerations. Symmetry aspects on the stability of superstructures and anti-phase boundaries have been discussed in [21,22].

The superstructures differ by the distribution of atoms over the Wyckoff positions. In the present work we used the FINDSYM program of Hatch and Stokes [23] in order to identify the corresponding space group (Table 1) and Wyckoff positions of all atoms in the superstructure. The sublattices of our primary interest are the La sublattice where the Sr atoms will substitute for La (in two concentrations: 12.5% and 50%) and the O sublattice where the vacancy will be considered. We will use the following abbreviations to refer to two compositions used in the present study: L87 for $La_{0.875}Sr_{0.125}Co_{0.25}Fe_{0.75}O_3$ and L50 for $La_{0.5}Sr_{0.5}Co_{0.25}Fe_{0.75}O_3$. It has been observed experimentally that the symmetry of $La_{1-x}Sr_xCo_{0.25}Fe_{0.75}O_{3-\delta}$ crystals changes with the Sr content [24–26]. The structural changes involve the symmetry reduction from rhombohedral to orthorhombic. At the same time, cubic symmetry can also be observed for high concentrations of Sr accompanied by high deviations from stoichiometry on the oxygen sublattice.

The symmetry changes are determined by the local site symmetry in the superstructure. The superstructures containing the sublattices in Fig. 1 have one Wyckoff position for La atoms. However, when one Sr atom (the case of L87) substitutes for La (Table 1) in a superstructure containing the sublattice A, the symmetry changes from cubic (Im-3 m) to rhombohedral (R-3 m); while superstructures containing the sublattices B and C, the symmetry changes from tetragonal (P4/mmm) to orthorhombic (Amm2 and Cmm2).

Table 1
Space groups of different superstructures containing sublattices from Figs. 1 and 2 with Co and Sr substitution in the cubic perovskite structure. LCFO, L87 and L50 stand for $LaCo_{0.25}Fe_{0.75}O_3$, $La_{0.875}Sr_{0.125}Co_{0.25}Fe_{0.75}O_3$ and $La_{0.5}Sr_{0.5}Co_{0.25}Fe_{0.75}O_3$, respectively. The most energetically favorable structures are indicated in bold.

Fig. 1	LCFO	L87	Fig. 2 (L50)		
			D	E	F
A	Im-3 m	R-3 m	Fmmm	P4/nmm	Pn-3 m
B	P4/mmm	**Amm2**	Pmma	1) P4/mmm 2) Pmm2	$P4_2/mcm$
C	P4/mmm	Cmm2	Pmna	**1)Pmma** 2) P4mm	P-4 m2

We start with the superstructures based on the Co/Fe sublattices depicted in Fig. 1 and consider the substitution of La atoms by four Sr atoms (the case of L50). There are six possible inequivalent arrangements for 4 Sr atoms in the cubic La sublattice, of which we consider here three for the reasons of formation of anti-phase boundaries as described above. With the aim of studying the energetically preferable configuration for L50 we have to consider all three La-Sr arrangements for each superstructure containing the sublattices from Fig. 1. Fig. 2 illustrates the three arrangements of Sr atoms on the La/Sr sublattice. All space groups for the superstructures from combinations of sublattices in Figs. 1 and 2 are collected in Table 1. It is also possible to have two space groups for one combination (sublattice E in Table 1). Two space groups are due to different orientations of the plane of Sr atoms in sublattice E with respect to the two Co atoms in sublattices B and C. Having determined the optimum structure for fixed stoichiometries on the Co/Fe and La/Sr sublattices, the oxygen vacancy can be tackled. We denote the concentration per site of oxygen vacancies by c_V. In our calculations on oxygen vacancy (V_O) in L50 and L87 only the supercell of 40 atoms giving $c_V = 12.5\%$ was chosen. The oxygen vacancy represented an F-center (neutral supercell).

In order to discuss all possible space groups for crystals with oxygen vacancies, let us mention that crystals with orthorhombic (Amm2) and tetragonal (Pmma) symmetry represent the ground state for L87 and L50, respectively (this will also be discussed quantitatively below). The 24 oxygen atoms in these crystals are distributed over 10 and 8 Wyckoff positions in L87 and L50, respectively. The symmetry of such crystals with V_O changes with the location of the vacant site. The space groups of crystals with one V_O per supercell are collected in Table 2. There are three space groups for L87 and two space groups for L50 with V_O. In the case of Sr 50%, the oxygen vacancy prefers to be further from the plane of Sr atoms. However, the two superstructures (Table 2) differ by the V_O - Co distance, too. It is at the shortest distance for the superstructure B + E. In the case of Sr 12.5%, the oxygen vacancy prefers to be far from Co atoms but near to a Sr atom. We expect on the basis of these results an importance of Sr and V_O clustering discussed in [27].

An analysis of energetic preference of different superstructures will be given in Section 4.1.

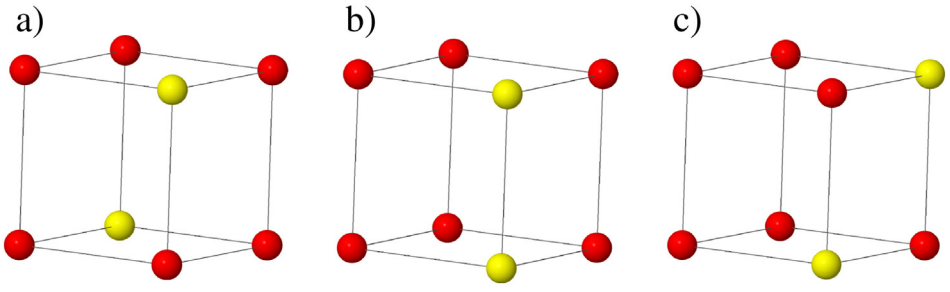

Fig. 1. The Fe atom sublattice in cubic 40 atoms supercell of LaFeO3 with three different possible arrangements of two Co atoms (yellow) replacing Fe atoms (red): a) sublattice A, b) sublattice B, c) sublattice C. (For interpretation of the references to colour in this figure legend, the reader is referred to the web version of this article.)

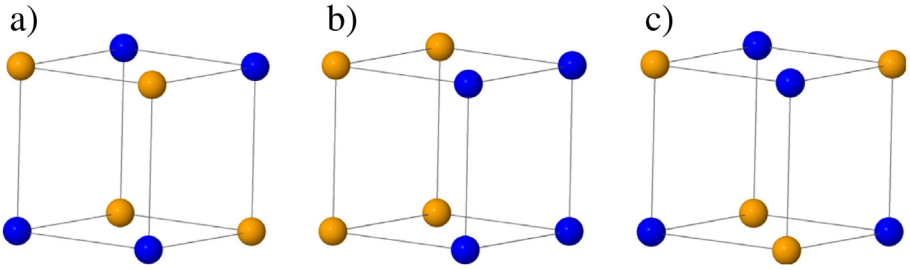

Fig. 2. The La atom sublattice in cubic 40 atoms supercell of LaFeO3 with three different possible arrangements of four Sr atoms (blue) replacing La atoms (orange): a) sublattice D, b) sublattice E, c) sublattice F. (For interpretation of the references to colour in this figure legend, the reader is referred to the web version of this article.)

3. Computational methods

3.1. Static lattice energies

For all the total energy calculations reported here we used the projector augmented wave (PAW) method [28] and scalar-relativistic pseudopotentials (PPs) substituted for 46 electrons on La, 18 electrons on Co, 12 electrons on Fe, 28 electrons on Sr and 2 electrons on O atoms. The exchange-correlation functional was that of Perdew, Burke and Ernzerhof [29] (PBE). The plane wave cut-off energy was fixed at 520 eV for the geometry optimization and increased to 600 eV for the phonon frequency calculations. The lattice parameters and internal coordinates were optimized until the energy difference was below 10^{-5} eV. The integrations in reciprocal space over the Brillouin zone were performed using a 4×4×4 Monkhorst-Pack scheme [30]. The electron occupancies were determined with the Gaussian method [31] using a smearing parameter of 0.2 eV. A ferromagnetic structure of $La_{1-x}Sr_xCo_{0.25}Fe_{0.75}O_{3-\delta}$ was assumed throughout all the spin-polarized calculations.

3.2. Vibrational contributions to free energy

The phonon contribution to the Helmholtz free energy is given within the harmonic approximation by the standard expression:

$$E_{vib}-TS_{vib} = k_BT\int_0^{\infty} F(\omega)\ln\left[2\sinh\left(\frac{\hbar\omega}{2k_BT}\right)\right]d\omega \quad (1)$$

In Eq. (1) $F(\omega)$ represents the phonon density of states, ω the phonon frequency and $\hbar$ the reduced Planck constant. In the present study the contribution of lattice vibrations to formation energies of oxygen vacancies in complex perovskite oxides is determined quantitatively using the direct method [32] to calculate phonon frequencies. The integral over the phonon density of states should be approximated by sampling over k-points in the first Brillouin zone.

Table 2
Space groups of L87 and L50 with one V_O per supercell at different Wyckoff positions. Only one superstructure with sublattice B for L87 and two superstructures 1) a combination of sublattices C and E, 2) a combination of sublattices B and E for L50 are chosen (see the text and Table 1). The most energetically favorable structures are indicated in bold.

Compound	Space group
L87: B	P1
	Amm2
	Pm
L50: C + E	**Pmm2**
	Pm
L50: B + E	**Pmm2**
	Pm

In our cases, the phonon frequencies were calculated within the harmonic approximation with the direct method as implemented in the VASP 5.2 code [33,34]. Since we used 40 atom supercells for both L50 and L87, the phonon contribution was determined at the Γ-point only. In the phonon calculations required for calibrating the chemical potential of oxygen (see below) we used MgO as a reliable reference material, since it is relatively easy to calculate its properties and those of Mg *ab initio*. However, as shown in [35], more than one k-point of the primitive unit cell would require calculating the free energy of a bulk crystal properly. To achieve a sampling of their phonon spectra we therefore use the same direct method with 3×3×3 supercells for hexagonal Mg and cubic MgO.

3.3. The contribution of vacancies

It is well known that the Sr^{2+} ion substituting for La^{3+} must be compensated by electronic defects (holes) or charged vacancies. The oxygen vacancies prevail over electronic defects at high temperatures [24,36]. The formation energy of V_O depends on the oxygen chemical potential, which has to be referred to the zero of energy that depends on the particular total energy method employed. To handle this we adopt, as described below, the method of Finnis et al. [37,38]. This is our favored approach because it makes use of experimental oxide heats of formation, thereby avoiding a calculation of the total energy of an oxygen molecule, which is known to be significantly overestimated in *ab initio* calculations with PBE. We thereby cancel the error in going from the molecule to the solid which originates from DFT error in both the molecular and solid-state calculations. Other strategies have been described in the literature to deal specifically with the problem of referencing the oxygen chemical potential [39].

The Gibbs free energy of formation of V_O as a function of temperature is calculated from:

$$\Delta G_F^0\left(T,p_{O_2}\right) = \left[E_{tot}^{V_O}+\left(E_{vib}^{V_O}-TS_{vib}^{V_O}\right)+pV^{V_O}\right]- \left[E_{tot}^{p}+\left(E_{vib}^{p}-TS_{vib}^{p}\right)+pV^{p}\right]+\mu_o\left(T,p_{O_2}\right), \quad (2)$$

where superscripts p, V_O stand for perfect and defective crystals, respectively, E_{tot} total electronic energy, E_{vib} the vibrational contribution to internal energy (including zero point vibrations), S_{vib} the entropy of vibrations, V the supercell volume, T the temperature, and p the pressure. The oxygen chemical potential $\mu_o(T,p_{O_2})$ was estimated following the approach discussed elsewhere [37,38], *viz.*

$$\begin{aligned}\mu_o\left(T,p_{O_2}\right) &= \mu_O^0(\mathrm{T})+\frac{1}{2}k_BT\ln\left(\frac{p_{O_2}}{p^0}\right)\\ &= E_{tot}^{AO}+\frac{1}{m}\left(E_{vib}^{AO}\left(T^0\right)-TS_{vib}^{AO}\left(T^0\right)\right)-E_{tot}^{A}\\ &-\frac{1}{l}\left(E_{vib}^{A}\left(T^0\right)-TS_{vib}^{A}\left(T^0\right)\right)-\Delta G^{AO}\left(T^0\right)+\Delta\mu_o(T)\\ &+\frac{1}{2}k_BT\ln\left(\frac{p_{O_2}}{p^0}\right),\end{aligned} \quad (3)$$

where $\mu_O^0(\mathrm{T})$ is the standard chemical potential, superscripts *AO* and *A* stand for the reference binary oxide, and its metal, respectively; in this

case we have used MgO. T^0 is equal in our case to standard state temperature 298.15 K. $\Delta G^{AO}(T^0)$ is the standard Gibbs free energy of formation, taken from a thermodynamic database [40], and our case we find $\Delta G^{MgO}(T^0) = 601.6$ kJ/mol. $\Delta\mu_o(T)$ is the difference in chemical potentials at the temperature of interest and standard state, which is also taken from the thermodynamic database [40]. k_B is Boltzmann's constant, p_{O_2} and p^0 are the oxygen partial pressure and standard pressure, respectively. The pre-factors $1/m$, $1/l$ in Eq. (3) represent the ratios of the number of atoms in the primitive unit cell to that in the supercell for binary oxide and metal, respectively, which for our case are both 1/27.

It is worth emphasizing the advantage here of avoiding direct calculations of O_2 molecule properties in the plane wave basis with the PBE functional [11]. In this case the calculated O_2 molecular binding energy deviates significantly from the experimental value (by > 1.5 eV) [11,41] which would have been an unacceptable source of error for the formation energy of V_O. The phonon contribution to ΔG_F from MgO and Mg in Eq. (2) at room temperature is given by

$$E^{AO}_{vib}\left(T^0\right) - TS^{AO}_{vib}\left(T^0\right) - E^{A}_{vib}\left(T^0\right) + TS^{A}_{vib}\left(T^0\right) \approx 0.14\text{eV}. \quad (4)$$

4. Results and discussion

4.1. Perfect superstructures and their energies

In the present study we used the orthorhombic symmetry for both L50 (space group Pmma) and L87 (space group Amm2) crystals. The crystals with this symmetry have the lowest calculated total energies in comparison to crystals with other symmetries from Table 1. The total energy difference for L87 is 0.88 eV per 40 atom supercell between the superstructures with Amm2 and R-3 m space groups and 0.56 eV between the superstructures with Amm2 and Cmm2 space groups. A comparison of cube root of lattice volume would be possible between the calculations and experiments [24]. Both the calculation and experiment agree that the volume decreases with Sr content. The calculated cube root of lattice volume for L87 and L50 is 3.88 and 3.86 Å, respectively. These values agree very well with the experimental ones, e. g. 3.89 and 3.87 Å, respectively.

Such a careful analysis of the symmetry changes for the fully relaxed structures is important for the phonon frequencies calculations in order to avoid the presence of imaginary frequencies. Then, the corresponding free energies can be calculated for the ground state structures.

The difference in total energy for L50 between the superstructure with the Pmma space group and all the others from Table 1 varies from 3.12 meV to 0.53 eV. The smallest difference in total energy is observed between the two symmetries for the combination of C and E superstructures (Table 1). We will use also the superstructure L50: B + E for comparison.

The size of a 40 atom supercell ($\delta = 0.125$) is convenient for L50 in view of the experimental stoichiometries of Tai et al. [24]. In these experiments the measured stoichiometry deviation was $\delta = 0.07$ for $La_{0.6}Sr_{0.4}Co_{0.2}Fe_{0.8}O_{3-\delta}$ and 0.14 for $La_{0.5}Sr_{0.5}Co_{0.5}Fe_{0.5}O_{3-\delta}$ at 1073 K and 10^{-1} bar. The oxygen vacancies in L50 may play an important role, being at least partly responsible for the decrease in electrical conductivity at high temperatures as shown, for example, by Tai et al. [24] and Bouwmeester et al. [36]. In contrast, the compound L87 is highly stoichiometric within a broad temperature range in air [24]. Deviations from stoichiometry of the order of 2% at the maximum are only expected at high temperatures. Similar stoichiometry deviations were seen in the experiments of Mizusaki et al. for $La_{0.9}Sr_{0.1}CoO_3$ [43] under the same conditions (see further discussion on these aspects in Section 4.3). These experimental results indicate higher formation energies of V_O for L87. We discuss further below the implications of these observations for the formation energy of V_O. Notice that the spin magnetic moment of Co increased in our calculations from 1.0 μ_B for L87 to 1.4 μ_B for L50.

4.2. Vibrational contribution to formation energies

In Fig. 3a the calculated free formation energy ΔG^0_F of V_O at standard oxygen pressure is given for both L50 (red curves) and L87 (black curves). The role of phonons is also demonstrated by calculating ΔG^0_F without the phonon contribution in the solid, i.e. when the temperature dependence is given by the chemical potential of oxygen only.

As expected ΔG^0_F is smaller for L50 in comparison to L87, in accordance with experimental findings. It is also the case even if the oxygen partial pressure of 10^{-8} atm is taken into account for L87 at so high concentration of vacancies as 12.5% (see Section 4.3 for details). The phonon contribution increases with T for both compounds. Moreover, the difference between ΔG^0_F's of the two compounds increases with T from 1.4 eV at 400 K to 1.9 eV at 1300 K. If, however, the phonon contribution in the solid is neglected, then the difference remains constant at all T (dashed curves). As also seen in Fig. 3a the sign of the phonon contribution to ΔG^0_F is different in the two compounds, being positive in L87 and negative in L50. Note that ΔG^0_F in Fig. 3a was calculated for the case of L50: C + E. The effect of phonons on ΔG^0_F may be different for other

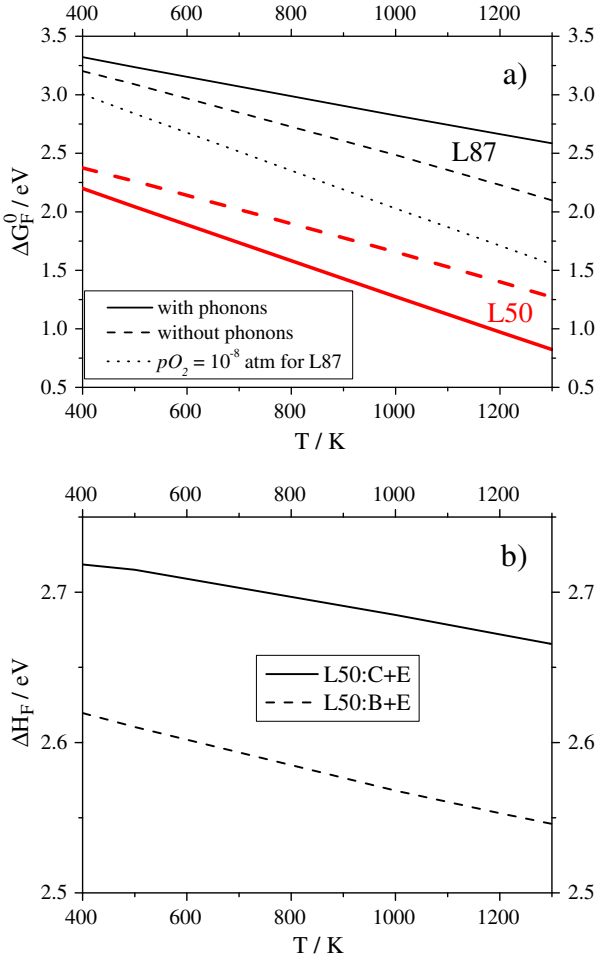

Fig. 3. (a) The free energy of formation ΔG^0_F per unit cell of V_O as a function of temperature, T, at standard oxygen pressure for L87 (solid black line) and L50 (solid red line, the combination of sublattices C and E). The dashed curves show the corresponding results without the phonon contributions. The dotted curve represents ΔG_F including the phonon contribution for L87 at oxygen partial pressure $p_{O_2} = 10^{-8}$ atm. (b) The enthalpy of formation of V_O for L50 as a function of T (with the phonon contribution included). (For interpretation of the references to colour in this figure legend, the reader is referred to the web version of this article.)

vacancies and/or superstructures. For example, the case of L50:B + E is characterized by an increase in ΔG_F^0 due to phonons (Fig. 4) similar to L87. Also, ΔG_F^0 for L50:B + E is close to that for L50:C + E if the phonon contribution in the solid is neglected. We conclude that for meaningful calculations of vacancy formation energies in complex oxides it is essential to choose the appropriate superstructures and to include the contribution of phonons. The free energies of formation with phonons for the two combinations in Fig. 4 differ by 0.67 eV at T = 1300 K. To better understand the effect of phonons for ΔG_F^0 in the two compounds (L87 and L50) and two combinations in Figs. 3 and 4, one could consider that the phonon contribution to ΔG_F^0 is mainly given by

$$\left(E_{vib}^{V_O} - TS_{vib}^{V_O}\right) - \left(E_{vib}^{p} - TS_{vib}^{p}\right) + \text{vibrational contribution to } \mu_o.$$

Since the vibrational contribution to μ_o is always the same, let us consider for simplicity the difference $\Delta = \left(E_{vib}^{V_O} - TS_{vib}^{V_O}\right) - \left(E_{vib}^{p} - TS_{vib}^{p}\right)$ only. In Fig. 5 this difference is plotted as a function of T. It is positive and increasing for L87 and L50:B + E but negative and decreasing for L50:C + E. We suggest this effect is the main reason for the observed importance of V_O in L50.

Calculating the formation enthalpy is relevant for a comparison to the experimental data (see Section 4.3). All entropy terms in Eqs. (2) and (3) are ignored in order to calculate the formation enthalpy ΔH_F. We estimated that ΔH_F for L87 is 3.7 eV and is almost temperature independent. As shown in Fig. 3b the dependence of ΔH_F on temperature is different for L50:B + E and L50:C + E.

In Fig. 6 the total phonon density of states is presented for all the three cases considered here. The L50 compounds are characterized by softer frequencies in comparison to L87. The L50:C + E compound has an increased phonon density in the range from 0 to 50 cm^{-1} in comparison to L87 and L50:B + E. Specifically in this range the softer phonons make a significant contribution to the free energy. The effect of soft frequencies is particularly important for high temperatures. According to our results, the contribution of a low frequency of 25 cm^{-1} to the free energy is 35 times the contribution of a high frequency of 612 cm^{-1} at T = 1000 K for L50:C + E with V_O. The main contribution to soft vibrational modes is due to O, La and Sr atoms. The Fe and Co atoms contribute at higher frequencies whereas the O atoms are involved at all frequencies.

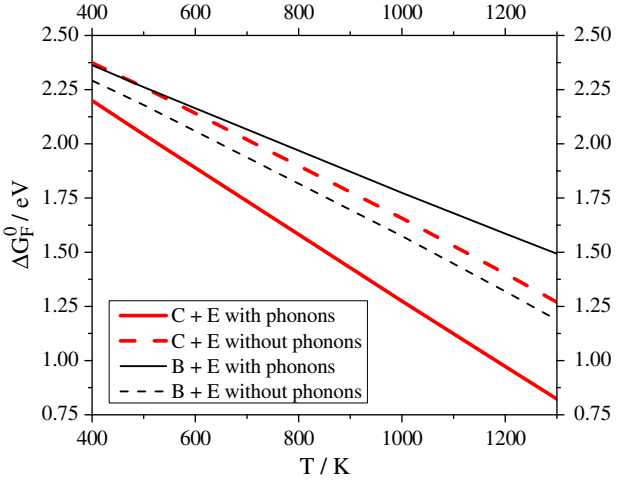

Fig. 4. The free formation energy per unit cell of V_O as a function of temperature, T, at standard pressure for two combinations of sublattices for L50 (bold and red curves for C and E, black curves for B and E). (For interpretation of the references to colour in this figure legend, the reader is referred to the web version of this article.)

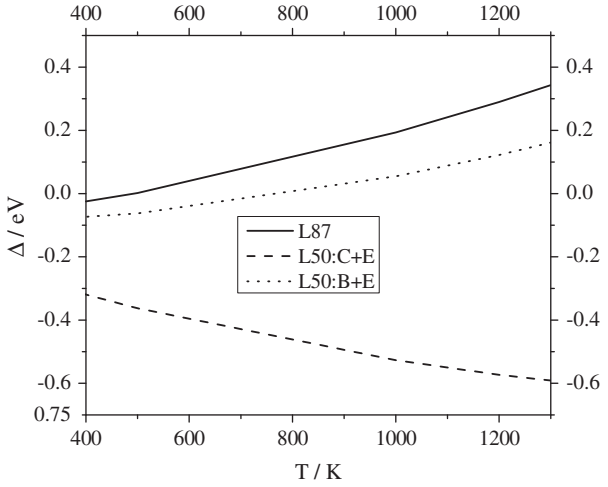

Fig. 5. The energy difference $\Delta = \left(E_{vib}^{V_O} - TS_{vib}^{V_O}\right) - \left(E_{vib}^{p} - TS_{vib}^{p}\right)$ as a function of T for L87 and L50.

4.3. A comparison to the experimental literature

Our estimates of ΔG_F^0 also illustrated the effect of varying oxygen partial pressure for L87 (Fig. 3a, dotted curve). According to the measurements [36] very low p_{O_2} (of the order of 10^{-8} atm) would be needed for the calculated vacancy concentration of $c_V = 12.5\%$. The calculated ΔG_F^0 then decreases from 2.82 eV (standard pressure) to 2.03 eV ($p_{O_2} = 10^{-8}$ atm) at T = 1000 K. An alternative comparison to results in the experimental literature can be made in terms of the enthalpies of formation, including the thermogravimetric measurements of Mizusaki et al. on (La,Sr)CoO_3 [42] and (La,Sr)FeO_3 [43]. In these measurements the partial molar enthalpy of oxygen Δh_o as a function of δ for different Sr concentrations was determined. The negative of this measured quantity is then equivalent to our calculated ΔH_F (Fig. 3b). Thus, $-\Delta h_o$ was 3.2 eV and 0.9 eV for $La_{0.9}Sr_{0.1}CoO_{3-\delta}$ and $La_{0.5}Sr_{0.5}CoO_{3-\delta}$, respectively. For $La_{0.9}Sr_{0.1}FeO_{3-\delta}$ $-\Delta h_o$ varies almost stepwise [43] between the oxidation states (4+/3+ and 3+/2+). In the experimental work [43] the values of 5.0 and 1.2 eV were estimated for the formation enthalpies. As discussed above the calculated value of ΔH_F for L87 is 3.7 eV and is, thus, close to the middle of the range for $La_{0.9}Sr_{0.1}FeO_{3-\delta}$ [43], i.e 3.1 eV. By contrast, the calculated average value of ΔH_F for L50:B + E and L50:C + E is 2.6 eV (see Fig. 3b) which is 1.7 eV larger than the measured one for $La_{0.5}Sr_{0.5}CoO_{3-\delta}$

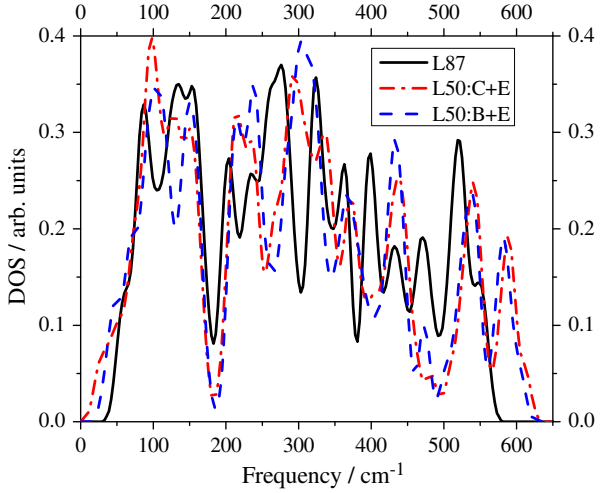

Fig. 6. The total phonon density of states (DOS) for L87 and L50 with V_O.

[42]. The Δh_o for $La_{0.4}Sr_{0.6}FeO_{3-\delta}$ and $La_{0.6}Sr_{0.4}FeO_{3-\delta}$ are roughly 1 eV. A similar oxidation enthalpy was measured by Bucher et al. [44] for $La_{0.4}Sr_{0.6}Fe_{0.4}Co_{0.6}O_{3-\delta}$. A comparison of the measured and calculated oxidation entropies $-T\Delta S_{ox}$, i.e. 1.06 eV for $La_{0.4}Sr_{0.6}Fe_{0.4}Co_{0.6}O_{3-\delta}$ from Ref. 44 vs. calculated value of 0.97 eV for L50:B + E at T = 1173 K, suggested no significant differences. However, the measured $-T\Delta S_{ox}$ for $La_{0.6}Sr_{0.4}FeO_{3-\delta}$ and $La_{0.4}Sr_{0.6}FeO_{3-\delta}$ [45] are smaller by 0.18 and 0.11 eV in comparison with the calculated value for L50:B + E. Recently, Kuhn et al. [46] measured the values $-T\Delta S_{ox}$ of the order of 0.66 eV for $La_{0.6}Sr_{0.4}FeO_{3-\delta}$. As seen in Fig. 3b the formation enthalpy for the two cases L50:B + E and L50:C + E differ by 0.12 eV. Note that we expect the formation enthalpy and free energy of formation to decrease by 0.3 eV when the supercell size changes from 40 atoms to 320 atoms as it was shown by Kotomin et al. [5] in their calculations on $Ba_{0.5}Sr_{0.5}Co_{0.75}Fe_{0.25}O_{3-\delta}$.

Note that we have undertaken specific permeability measurements and hybrid DFT functionals calculations to further compare the calculated formation energies to experiments which will be discussed in detail in a future paper [47].

5. Conclusions

1) In the present study a careful symmetry analysis has been performed for different Sr atoms and oxygen vacancy V_O arrangements in supercells of $La_{1-x}Sr_xCo_{0.25}Fe_{0.75}O_{3-\delta}$ with x = 0.125 and 0.5. Such defective crystals with V_O are characterized by orthorhombic and monoclinic symmetries.
2) From DFT calculations we find the lowest energy structure to be orthorhombic, independently of x.
3) The Gibbs free energy and enthalpy of formation of V_O were calculated as a function of temperature. We have estimated quantitatively the phonon contributions by calculating the phonon frequencies in defective and perfect $La_{1-x}Sr_xCo_{0.25}Fe_{0.75}O_3$ and included the contribution of the oxygen chemical potential. The concentration of oxygen vacancies was fixed at 12.5%.
4) We have shown that the lattice vibrations (phonons) play a significant role in determining the equilibrium concentration of oxygen vacancies in $La_{1-x}Sr_xCo_{0.25}Fe_{0.75}O_3$. The magnitude of the phonon contribution increases not only with temperature but also with Sr content. Its value can be as high as 0.5 eV for the concentration of Sr 50% at T = 1000 K. In this case we have shown that the strong dependence of vacancy formation energy on temperature can be attributed to phonons as much as to the oxygen chemical potential, and can take either sign, depending on the structure.
5) A careful comparison of formation enthalpies of V_O to the available experimental data from the literature (which included (La,Sr)CoO_3 and (La,Sr)FeO_3 [42,43]) suggested good qualitative agreement for the concentration of Sr 12.5%. Further investigations on this comparison are needed for higher concentration of Sr. However, the oxidation entropies for x = 0.5 as given by the phonons are very well reproduced in comparison to the experimental literature.

Acknowledgements

The research leading to these results received partial support from the EC GREEN-CC FP7 project 608524 and Latvian republic grant 237/2012. D.G. also thanks the HPC-Europa2 initiative of the European Commission and the Thomas Young Centre for financial support of his visit to Imperial College London. The authors thank the IT team of EPCC in Edinburgh for technical support and Evgeny Blokhin for help with plotting the graphs. Authors are grateful to Rotraut Merkle, David Fuks, Dane Morgan and Eugene Heifets for helpful discussions.

References

[1] J. Sunarso, S. Baumann, J.M. Serra, W.A. Meulenburg, S. Liu, Y.S. Lin, J.C. Diniz da Costa, J. Membr. Sci. 320 (2008) 13.
[2] C. Sun, R. Hui, J. Roller, J. Solid State Electrochem. 14 (2010) 1125;
A. Chroneos, B. Yildiz, A. Tarancón, D. Parfitt, J.A. Kilner, Energy Environ. Sci. 4 (2011) 2774.
[3] Y. Choi, M.C. Lin, M. Liu, J. Power Sources 195 (2010) 1441.
[4] S. Piskunov, E.A. Heifets, T. Jacob, E.A. Kotomin, D.E. Ellis, E. Spohr, Phys. Rev. B 78 (R) (2008) 121406.
[5] E.A. Kotomin, Yu.A. Mastrikov, M.M. Kuklja, R. Merkle, A. Roytburd, J. Maier, Solid State Ionics 188 (2011) 1.
[6] Yu.A. Mastrikov, M.M. Kuklja, E.A. Kotomin, J. Maier, Energy Environ. Sci. 3 (2010) 1544.
[7] Y.-L. Lee, J. Kleis, J. Rossmeisl, Y. Shao-Horn, D. Morgan, Energy Environ. Sci. 4 (2011) 3966.
[8] M. Pavone, A.M. Ritzmann, E.A. Carter, Energy Environ. Sci. 4 (2011) 4933.
[9] C. Wessel, M.-W. Lumey, R. Dronkowski, J. Membr. Sci. 366 (2011) 92.
[10] L.M. Petkovic, V. Utgikar, S.N. Rashkeev, J. Phys. Chem. C 115 (2011) 8709.
[11] Y.-L. Lee, J. Kleis, J. Rossmeisl, D. Morgan, Phys. Rev. B 80 (2009) 224101.
[12] P.G. Sundell, M.E. Björketun, G. Wahnström, Phys. Rev. B 73 (2006) 104112.
[13] R.A. Evarestov, E. Blokhin, D. Gryaznov, E.A. Kotomin, J. Maier, Phys. Rev. B 83 (2011) 134108.
[14] R.A. Evarestov, A.V. Bandura, J. Comp. Chem. 33 (2012) 1123.
[15] D. Gryaznov, R.A. Evarestov, J. Maier, Phys. Rev. B 82 (2010) 224301.
[16] D. Gryaznov, E. Blokhin, A. Sorokine, E.A. Kotomin, R.A. Evarestov, A. Bussmann-Holder, J. Maier, J. Phys. Chem. C 117 (2013) 13776.
[17] R.A. Evarestov, Quantum Chemistry of Solids, Springer, Heidelberg, 2007.
[18] A. Weizman, D. Fuks, E.A. Kotomin, D. Gryaznov, Solid State Ionics 230 (2013) 32.
[19] D. Fuks, L. Bakaleinikov, E.A. Kotomin, J. Felsteiner, A. Gordon, R.A. Evarestov, D. Gryaznov, J. Maier, Solid State Ionics 177 (2006) 217.
[20] E.M. Lifshitz, J. Phys. 7 (1942) 61;
E.M. Lifshitz, J. Phys. 7 (1942) 251.
[21] L.D. Landau, E.M. Lifshitz, Statistical Physics, 3rd Revised and Enlarged edition Elsevier, Oxford, 1980.
[22] A.G. Khachaturyan, Theory of Structural Transformations in Solids, Wiley, New York, 1983.
[23] H.T. Stokes, D.M. Hatch, J. Appl. Cryst. 38 (2013) 237(http://stokes.byu.edu/findsym.html).
[24] L.-W. Tai, M.M. Nasrallah, H.U. Anderson, D.M. Sparlin, S.R. Sehlin, Solid State Ionics 76 (1996) 273.
[25] S. Hashimoto, Y. Fukuda, M. Kuhn, K. Sato, K. Yashiro, J. Mizusaki, Solid State Ionics 181 (2010) 1713.
[26] K. Świerczek, B. Dabrowski, L. Suescun, S. Kolesnik, J. Solid State Chem. 182 (2008) 280.
[27] E.V. Tsipis, E.N. Naumovich, M.V. Patrekeev, A.A. Yaremchenko, I.P. Marozau, A.V. Kovalevsky, J.C. Waerenborgh, V.V. Kharton, Solid State Ionics 192 (2011) 42.
[28] G. Kresse, D. Joubert, Phys. Rev. B 59 (1999) 1758.
[29] J.P. Perdew, K. Burke, M. Ernzerhof, Phys. Rev. Lett. 77 (1996) 3865.
[30] J. Monkhorst, J.D. Pack, Phys. Rev. B 13 (1976) 5188.
[31] G. Kresse, J. Furthmüller, Phys. Rev. B 54 (16) (1996) 11169.
[32] G. Grimvall, Thermophysical Properties of Materials, North-Holland, Amsterdam, 1986.
[33] G. Kresse, J. Furthmüller, Comp. Mater. Sci. 6 (1996) 15.
[34] G. Kresse, J. Furthmüller, VASP the Guide, University of Vienna, Vienna, 2009. (http://cms.mpi.univie.ac.at/VASP/).
[35] A.V. Bandura, R.A. Evarestov, J. Comp. Chem. 33 (2012) 1554.
[36] H.J. Bouwmeester, M.W. Den Otter, B.A. Boukamp, J. Solid State Electrochem. 8 (2004) 599.
[37] M.W. Finnis, A.Y. Lozovoi, A. Alavi, Annu. Rev. Mater. Res. 36 (2005) 167.
[38] J. He, R.K. Behera, M.W. Finnis, X. Li, E.C. Dickey, S.R. Phillpot, S.B. Sinnot, Acta Mater. 55 (2007) 4325.
[39] L. Wang, Th. Maxisch, G. Ceder, Phys. Rev. B 73 (2006) 195107.
[40] NIST, NIST Chemistry Webbook, NIST, 2010. (http://webbook.nist.gov/chemistry/).
[41] D. Bocharov, D. Gryaznov, Yu.F. Zhukovskii, E.A. Kotomin, J. Nucl. Mater. 416 (2011) 200.
[42] J. Mizusaki, Y. Mima, S. Yamauchi, K. Fueki, J. Solid State Chem. 80 (1989) 102.
[43] J. Mizusaki, M. Yoshihiro, S. Yamauchi, K. Fueki, J. Solid State Chem. 67 (1987) 1.
[44] E. Bucher, W. Sitte, G.B. Caraman, V.A. Cherepanov, T. Aksenova, M.V. Ananyev, Solid State Ionics 177 (2006) 3109.
[45] J. Mizusaki, M. Yoshihiro, S. Yamauchi, K. Fueki, J. Solid State Chem. 58 (1985) 257.
[46] M. Kuhn, S. Hashimoto, K. Sato, K. Yashiro, J. Mizusaki, Solid State Ionics 195 (2011) 7.
[47] D. Gryaznov, S. Baumann, E. A. Kotomin (to be submitted).